Author Manuscript

Author Manuscript

Author Manuscript

Author Manuscript

HHS Public Access

Author manuscript

Science. Author manuscript; available in PMC 2019 March 22.

Published in final edited form as:

Science. 2018 August 31; 361(6405): . doi:10.1126/science.aao3048.

Cancer mutations and targeted drugs can disrupt dynamic signal encoding by the Ras-Erk pathway

L. J. Bugaj[1,*], **A. J. Sabnis**[2,3], **A. Mitchell**[1,†], **J. E. Garbarino**[4], **J. E. Toettcher**[1,‡,§], **T. G. Bivona**[1,3,5,§], and **W. A. Lim**[1,3,4,6,§]

[1]Department of Cellular and Molecular Pharmacology, University of California, San Francisco, San Francisco, CA 94158, USA.

[2]Department of Pediatrics, University of California, San Francisco, San Francisco, CA 94158, USA.

[3]Helen Diller Family Comprehensive Cancer Center, University of California, San Francisco, San Francisco, CA 94158, USA.

[4]Howard Hughes Medical Institute, University of California, San Francisco, San Francisco, CA 94158, USA.

[5]Division of Hematology and Oncology, University of California, San Francisco, San Francisco, CA 94158, USA.

[6]Center for Systems and Synthetic Biology, University of California, San Francisco, San Francisco, CA 94158, USA.

Abstract

The Ras-Erk (extracellular signal-regulated kinase) pathway encodes information in its dynamics; the duration and frequency of Erk activity can specify distinct cell fates. To enable dynamic encoding, temporal information must be accurately transmitted from the plasma membrane to the nucleus. We used optogenetic profiling to show that both oncogenic B-Raf mutations and B-Raf inhibitors can cause corruption of this transmission, so that short pulses of input Ras activity are distorted into abnormally long Erk outputs. These changes can reshape downstream transcription

§ Corresponding author.: wendell.lim@ucsf.edu (W.A.L.); toettcher@princeton.edu (J.E.T.); trever.bivona@ucsf.edu (T.G.B.).
*Present address: Department of Bioengineering, University of Pennsylvania, Philadelphia, PA 19104, USA.
†Present address: Program in Systems Biology, University of Massachusetts Medical School, Worcester, MA 01655, USA.
‡Present address: Department of Molecular Biology, Princeton University, Princeton, NJ 08544, USA.

Author contributions: L.J.B., J.E.T., T.G.B., and W.A.L. designed the study and experiments. L.J.B and J.E.T. generated cell lines. L.J.B, A.J.S., J.E.G., and J.E.T. performed Western blots. L.J.B. and J.E.T. performed and analyzed live-cell microscopy. L.J.B. designed and built the optoPlate, developed optoPlate assays, and performed and analyzed all optoPlate- based experiments. L.J.B. and A.M. developed and analyzed protocols for proliferation experiments. W.A.L. and T.G.B. oversaw and guided the project. L.J.B. and W.A.L. wrote the manuscript with an early draft by J.E.T. Manuscript review and editing was provided by all authors.

Competing interests: A patent application (U.S. provisional patent application no. 62/362,768) has been filed on the design of the optoPlate device.

Data and materials availability: All data needed to evaluate the conclusions in the paper are present in the paper or the supplementary materials.

SUPPLEMENTARY MATERIALS
www.sciencemag.org/content/361/6405/eaao3048/suppl/DC1
Figs. S1 to S13
Table S1

Author Manuscript Author Manuscript Author Manuscript Author Manuscript

and cell fates, resulting in improper decisions to proliferate. These findings illustrate how altered dynamic signal transmission properties, and not just constitutively increased signaling, can contribute to cell proliferation and perhaps cancer, and how optogenetic profiling can dissect mechanisms of signaling dysfunction in disease.

Signaling through the Ras-Erk (extracellular signal-regulated kinase) pathway controls diverse cell decisions, including survival, differentiation, and proliferation (1). A cell's fate is determined in part by the dynamics of Ras-Erk signals, which can be encoded by different receptors or cellular contexts (Fig. 1A) (2–6). Thus, the cell must be able to accurately transmit dynamic signal patterns and then decode them to make proper decisions (7–15). To understand how the cell transmits and decodes dynamic information, we recently developed optogenetic methods with which to interrogate cells with precisely controlled Ras inputs (Fig. 1B) (16). Our study revealed that the Ras-Raf-Mek-Erk protein kinase cascade acts as a high-fidelity transmission system, accurately transmitting dynamic signals with time scales ranging from minutes to hours to the nucleus [through nuclear localization of phosphorylated Erk (ppErk)] (Fig. 1A). In turn, downstream transcriptional networks then decode and integrate Erk dynamics to yield distinct cellular responses (2, 16–19).

Given the functional importance of Ras-Erk dynamics, we realized that changes in how the pathway transmits and decodes signals could potentially lead to cellular malfunction and disease. Mutations within the Ras-Erk pathway underlie a large proportion of human tumors (20), and these mutations are commonly thought to drive cancer phenotypes through constitutive proliferative signaling. However, cancer phenotypes might also result from the corruption of proper dynamic signal transmission and decoding. Such changes could result in misinterpretation of dynamic environmental signals that might, for example, instruct cells to proliferate in response to normally nonproliferative inputs. Detecting potential defects in signal transmission and filtering requires appropriate tools that have only recently become available. We applied optogenetic profiling to identify alterations in Ras-Erk signaling dynamics within cancer cells, and we showed how these changes can result in inappropriate cellular decision-making.

Optogenetic profiling of Ras-Erk signal transmission in lung cancer cells

We examined Ras-Erk signaling in five patient- derived non-small cell lung cancer (NSCLC) cell lines with endogenous, validated oncogenes in the Ras-Erk pathway [in the epidermal growth factor receptor (EGFR), Ras, and B-Raf] (Cell lines and putative driver mutations are listed in table S1). As controls, we examined two normal human lung epithelial cell lines (Beas2B and 16HBE) and mouse NIH 3T3 fibroblasts. To probe how these cells processed dynamic Ras signals, we transduced each cell line with optoSOS, a genetically encoded light-activatible probe for toggling Ras activity in living cells (Fig. 1B). The optoSOS system relies on the light-dependent dimerization of PhytochromeB (PhyB) and phytochrome-interacting factor 6 (PIF), which associate when exposed to red (650 nm) light and dissociate when exposed to far-red (750 nm) light. PhyB was tethered to the membrane, and PIF, fused to the Ras-activating Son of Sevenless Homolog 2 (SOS2) catalytic domain (SOS2cat), was expressed in the cytoplasm. Therefore, light could be used to reversibly

Author Manuscript Author Manuscript Author Manuscript Author Manuscript

recruit SOS2cat to the membrane and thus dynamically modulate Ras activity. We tracked signal transmission from Ras to Erk through live-cell microscopy by co-expressing a blue fluorescent protein (BFP)-Erk2 reporter, which accumulates in the nucleus upon activation (Fig. 1C) (21). For more high- throughput and long-term analysis, we developed the optoPlate, a device for optogenetic illumination in microwell plates (Fig. 1C and fig. S1). This device allowed us to stimulate cells dynamically across a large parameter space and analyze multiple cellular outputs over time through fixed-cell fluorescence microscopy.

Identification of cancer cell line with substantially altered Ras-Erk signaling dynamics

One of the five lung cancer cell lines, H1395, had altered dynamic signal transmission properties (analysis of all the cancer cell lines is provided in fig. S2, A and B). When H1395 cells were subjected to various pulsatile optoSOS activation patterns, Erk activity (BFP-Erk2 nuclear localization) responded sluggishly whenever we switched optoSOS on or off (Fig. 2A). In particular, Erk activity took longer to diminish after optoSOS was switched off: The deactivation half-life ($t_{1/2}$) of Erk in H1395 cells was ~20-fold longer than that observed in normal NIH 3T3 control cells (H1395 $t_{1/2}$ = 21 min; NIH 3T3 $t_{1/2}$ = 1 min). We confirmed these slow dynamics by means of Western blot for ppErk (Fig. 2B and fig. S3A). Thus, in H1395 cells, instead of switching off immediately after Ras input stops, Erk continues to signal.

The slow responsiveness and decay of Erk activity may degrade the H1395 cell's ability to resolve distinct high-frequency dynamic patterns of Ras stimulation. We applied optoSOS pulse trains that resemble naturally observed pathway dynamics (2–4) to normal lung epithelial cells (16HBE) and H1395 cancer cells. Both cell types resolved input pulses spaced far apart (at 40-min intervals) (Fig. 2C and fig. S3B). However, as the input pulses were spaced progressively closer, the H1395 cells failed to distinguish the higher- frequency pulses. Ultimately, the H1395 cells failed to perceive gaps in the signal and produced a constant Erk response (Fig. 2C, *5'* OFF condition). Thus, compared with normal cells, H1395 cells have an impaired ability to perceive dynamic pathway input (Fig. 2D).

B-Raf P-loop mutation (G469A) slows kinetics of signal decay

The H1395 cell line harbors a B-Raf G469A mutation. We thought that the slow OFF-kinetics of Erk could be caused by either defects in switching off Erk or Mek (such as defects in downstream phosphatase function) or by defects in switching off the mutant B-Raf. To find nodes in the pathway that may cause the slow dynamics, we repeated our optoSOS stimulation studies, but when switching off optoSOS, we also added inhibitors to block particular steps in the pathway—either the Mek inhibitor U0126 (which rapidly shuts off signal flow from Mek to Erk) or mutant B-Raf inhibitor PLX-8394 (which rapidly shuts off signal flow from mutant B-Raf to Mek) (Fig. 3A and fig. S4A) (22). When either of these inhibitors was added concurrently with optoSOS inactivation in H1395 cells, active phospho-Erk (ppErk) decayed rapidly (Fig. 3A and fig. S4B), suggesting that normal Mek and Erk dephosphorylation activity was intact and that the source of extended signal decay

Author Manuscript Author Manuscript Author Manuscript Author Manuscript

lay upstream. Together, these experiments indicated that slow ppErk OFF-kinetics might emanate from mutant B-Raf.

To further test whether the mutant B-Raf accounted for the slow OFF-kinetics of the pathway, we performed optogenetic profiling in which we linked the light-induced input to a different node. We used an optogenetic tool called optoBRaf. OptoBRaf is activated through inducible membrane recruitment of PIF fused to wild-type B-Raf, which stimulates its signaling to endogenous Mek (Fig. 3A, bottom) (23). OptoBRaf enabled us to stimulate the H1395 cells in a manner that bypassed the B-Raf G469A mutant. We observed rapid ppErk deactivation kinetics with optoBRaf stimulation, which was again consistent with a model in which the B-Raf G469A mutant is directly responsible for the altered pathway dynamics (Fig. 3A, bottom, and fig. S4C). This experiment produced a rebound in ppErk signal after the initial rapid decay. This may be caused by relief of negative feedback of ppErk onto mutant B-Raf (24, 25) because repeating this experiment in the presence of PLX-8394 eliminated this rebound. We also observed extension of Ras-Erk kinetics in Beas2B normal lung epithelial cells (lacking endogenous mutations in Ras, Raf, Mek, or Erk) engineered to express exogenous B-Raf G469A, and this extension was reversed in the presence of the B-Raf inhibitor PLX-8394 (fig. S4, D, E and F). Together, these results implicate the mutant B-Raf G469A as a kinetics-altering node in H1395 cancer cells.

Lagging pathway kinetics of B-Raf G469A mutants were specific to mutation position because another member of our cancer cell panel— HCC364—carried a B-Raf V600E mutation and showed wild-type, fast pathway kinetics (fig. S2B). G469 lies in the P-loop of B-Raf, which normally associates with the activation loop to maintain the B-Raf kinase domain in an inactive, auto- inhibited conformation (26). Normal activation of B-Raf requires release of this auto-inhibition, which both frees the kinase domain and promotes the activating homo- or heterodimerization of B-Raf. Oncogenic P-loop mutations both disrupt the inactive conformation and enhance dimerization of B-Raf (26–28). Several P-loop mutations impair B-Raf activity yet can also be oncogenic, likely because they enhance C-Raf transactivation through B-Raf-C-Raf dimerization (26).

Enhanced B-Raf dimerization induced by the P-loop G469A mutation might also cause the delayed OFF-kinetics. If so, delayed OFF-kinetics should be reversed in the presence of mutations that disrupt B-Raf dimerization, such as the R509H mutation (29, 30). Indeed, Beas2B cells transiently transfected with *BRAF* G469A showed elongated ppErk decay kinetics, whereas cells transfected with the *BRAF* G469A/R509H double mutant showed wild-type kinetics (fig. S5).

Other B-Raf P-loop mutant lines would also be expected to show extended ppErk inactivation kinetics. Indeed, we searched for additional lung cancer cell lines driven by B-Raf P-loop mutations and found that they also showed slow ppErk response to input Ras pulses (fig. S6A). Specifically, the Cal12T and H1666 lung cancer cell lines, each expressing endogenous B-Raf G466V (a distinct oncogenic P-loop mutation from G469A), showed a similar sluggish response. As in H1395 cells, this slowed response was reversed in the presence of the Raf inhibitor PLX-8394. Unlike the activating G469A mutation, G466V decreases catalytic activity (26). Nevertheless, both mutants extended Ras-induced ppErk

Author Manuscript Author Manuscript Author Manuscript Author Manuscript

kinetics, which may reflect their shared propensity for enhanced dimerization with C-Raf. Although we readily found examples of altered kinetics in *BRAF*-mutant cells, a screen of cell lines with diverse Ras mutants revealed no similar examples (fig. S7, A and B), suggesting that B-Raf is a more sensitive point for altering ppErk signaling dynamics.

Paradox-activating drugs that perturb B-Raf dimerization also alter Ras-Erk kinetics

Drugs that enhance B-Raf homo- or heterodimerization would also be expected to yield extended Erk inactivation kinetics. We therefore examined ppErk kinetics in the presence of so- called paradox-activating B-Raf inhibitors. Although designed to inhibit mutant B-Raf activity, this family of drugs paradoxically activates Raf- Mek-Erk signaling by enhancing B-Raf dimerization with C-Raf (29, 31, 32). This paradoxical pathway activation can actually stimulate cancer formation in certain patients receiving these drugs (33–36). We found that both vemurafenib and SB590885—two B-Raf inhibitors in this class-extended the otherwise fast Erk kinetics in both wild-type fibroblasts (Fig. 3B) and Beas2B lung epithelial cells (fig S6B). Although mechanistically similar, vemurafenib and SB590885 are chemically distinct and had differing dose-dependent effects on ppErk signal kinetics (fig. S8). By contrast, the B-Raf inhibitor PLX-8394, which does not enhance Raf dimerization, had no effect on Erk kinetics. As with G469A mutant-extended kinetics, drug-extended kinetics were reversed with Mek inhibition, indicating that the drugs extended kinetics through a mechanism upstream of Mek activation (fig. S9).

Increasing Raf dimerization with B-Raf inhibitors can enhance active Ras nanocluster formation, resulting in increased gain between Ras and Erk but no change in the dynamics of nanocluster formation (37, 38). Our results confirm increased gain from Ras to Erk (fig. S8) and are thus consistent with this mechanism. Further, because slow ppErk kinetics emerge despite fast Ras nanocluster decay dynamics (38), we conclude that the sustained ppErk signal originates downstream of Ras activation and cluster formation at the level of Raf activation. In total, these data support a model in which B-Raf P-loop mutations that enhance homo- or heterodimerization cause a lag in the dynamics of shutting off overall Raf activity (Fig. 3C).

Modeling how slow Ras-Erk dynamics could alter cell decisions

We examined how such altered Ras-Erk transmission properties could affect downstream cellular decision-making. Changes in the dynamic response of the Ras-Erk pathway fundamentally change how the cell filters dynamic inputs. The wildtype Ras-Erk pathway filters signals shorter than ~4 min (the pathway loses ability to transmit more transient changes) while faithfully transmitting longer ones ranging from minutes to hours (16). To examine the consequences of changing these filtering parameters, we constructed a simple model that integrates a low-pass filter with downstream transcription and resultant cell fate commitment (fig. S10A). In this model, the cell senses whether the intensity of a ppErk signal rises above an activation threshold, above which ppErk-dependent transcription begins (fig. S10B).

Author Manuscript Author Manuscript Author Manuscript Author Manuscript

We compared this system with fast (normal) and slow system responses. In the model, slowing the system response can sustain otherwise transient signal activity in response to dynamic inputs (fig. S10B). In particular, pulse trains of short pulses were poorly resolved and interpreted as a stronger, more continuous input. Over a sufficiently long integration time, cellular decisions for downstream outputs such as gene expression and proliferation could differ substantially between the fast and slow pathway models (fig. S10, C and D).

Because oncogene- and drug-extended kinetics are often accompanied by increased basal signaling (figs. S4, E to F; S6B; S8; and S9), we examined the effects of increased basal signaling by changing the activation threshold in our model. Increased basal signaling is equivalent to a lower activation threshold. In the model, although increased basal signaling (lower threshold) minimally sensitized cells to proliferate under fast ppErk kinetics, slow ppErk kinetics dramatically increased the proliferative response (fig. S10D). Thus, although increased signaling and extended kinetics may synergize to control cellular response, our model predicts that kinetics can have a dominant role in downstream cellular behavior.

Slow pathway dynamics alter transcriptional responses

To experimentally test whether changes in signal transmission dynamics could alter gene expression decisions in cells, we measured the amounts of several downstream output proteins in response to optoSOS inputs. We sought an experimental model in which we could isolate the effects of altered Ras-Erk kinetics in a well-controlled cell line that lacks potentially confounding mutations. Thus, we compared the responses of wild-type NIH 3T3 cells in the presence and absence of 100 nM SB590885 (paradox inhibitor of B-Raf). This concentration of drug extended Ras-Erk pathway decay kinetics and minimally increased basal ppErk levels (figs. S8, A and B, and S11A). Cells were seeded and serum-starved in 384-well plates and, in the presence or absence of drug, exposed to various dynamic input patterns with the optoPlate (Fig. 4A and fig. S11B). After stimulating the cells over several hours, cells were fixed and immuno- stained for Erk-dependent transcriptional targets.

We measured the expression of two immediate early gene targets, cJun and early growth response protein 1 (EGR1), and the cell-cycle regulator Cyclin D1 (Fig. 4A). These are targets that show strong dependence on the dynamics of input signals. In normal NIH 3T3s, cJun and Cyclin D1 expression are strongly induced with continuous optoSOS stimulation and are not induced by pulsatile, transient stimulation. By contrast, EGR1 shows a peak of expression with continuous stimulation but then shows an adaptive decrease in expression, potentially mediated by negative feedback (39). EGR1 expression stayed higher with pulsed stimulation (30 min on, 30 min off), probably because such pulsatile stimulation prevents the accumulation of maximal negative feedback (Fig. 4B and fig. S11, C to H).

These dynamically responsive Ras-Erk gene targets showed changes in regulation with altered Ras-Erk signal transmission. In all cases, when we performed dynamic stimulation studies in the presence of the drug SB590885, the pulsed-input response shifted to more closely resemble that of the normal constant-input response. Upon SB590885 addition, both cJun and Cyclin D1 accumulated in response to normally subthreshold pulsed stimulation. Conversely, pulsed stimulation in the presence of SB590885 yielded the adaptive response of

Author Manuscript Author Manuscript Author Manuscript Author Manuscript

EGR1 normally observed with a constant Ras input (Fig. 4B and fig. S11, C to H). Together, these results show that altering Ras-Erk transmission kinetics can change how cells filter dynamic signals, altering expression patterns of the genes that control important cell decisions.

Slow pathway dynamics shift thresholds for inducing proliferation

Because the Ras-Erk pathway is a key driver of proliferation, and because we observed differential expression of the cell-cycle regulator Cyclin D1, we tested whether slowed Ras-Erk transmission kinetics might corrupt proper control of proliferation by driving cell-cycle entry in response to what are normally nonproliferative dynamic input patterns. Dynamic Erk signals are linked to cell-cycle control in vivo, but the physiological parameters of Erk dynamics are not well defined (2–4, 40). We therefore tested how cells responded to a range of dynamic Ras inputs, both in the presence and absence of SB590885-induced delay in ppErk kinetics. We examined a set of signal patterns that, after 19 hours of stimulation, could drive cell-cycle entry, as assayed by means of DNA incorporation of 5-ethynyl-2-deoxyuridine (Edu) during S-phase (Fig. 4C and fig. S12, A, B, and C). Cells in each microwell received either no signal, a constant signal, or a periodic signal. The time in the ON phase (ON interval) and OFF phase (OFF interval) of the periodic signal was systematically varied between microwells.

The resulting heatmap of proliferation as a function of the dynamic stimulation pattern is shown in Fig. 4C (no-signal and constant-signal conditions are depicted in fig. S12D; heatmaps are shown in Fig. 4C and fig S12E). In normal 3T3s, we delineated a “growth regime” of input signals that drive the strongest proliferation. This showed that Ras-Erk-induced cell-cycle entry required strong and sustained signals: those largely consisting of long ON intervals separated by short OFF intervals. Slowing Ras-Erk transmission kinetics with drug dramatically expanded this growth regime, increasing proliferation across a range of otherwise nonproliferative Ras input patterns (Fig. 4C and figs. S12F and S13).

Conclusion: Mutants that alter how a cell perceives signals can contribute to disease

Some cancer mutations or targeted drugs can alter a cell’s dynamic signal transmission and filtering properties, and such changes can reshape how a cell perceives or misperceives its environment, potentially contributing to disease phenotypes (Fig. 4D). Such signal misinterpretation might contribute to hyperproliferation, but Ras-Erk signaling functions in many cell behaviors, including cell survival and migration, and thus defective signal transduction may plausibly affect these behaviors in disease as well. Functional profiling of intact signaling networks with optogenetics provides a powerful method with which to uncover and understand such alterations in cellular decision-making (41). We anticipate that profiling more cancers and more pathways in this manner may uncover other types of dynamic signaling phenotypes that could contribute to disease. The improved understanding we gain of how mutated signaling networks differentially process information may help us mechanistically understand cancer, autoimmunity, and other diseases that involve corrupted

Author Manuscript Author Manuscript Author Manuscript Author Manuscript

cellular decision-making and may provide new dynamically optimized strategies for targeting these diseases (42–44).

Materials and Methods *Plasmid constructs, viral packaging, and transduction*

OptoSOS components Phy-mCh-CAAX (Addgene # 50839), YFP-PIF-SOS2cat (Addgene # 50851), and BFP-Erk2 (Addgene # 50848) were described previously (16, 45). Phy-mCh-CAAX used the KRas4B-derived CAAX sequence KMSKDGKKK- KKKAKTKCVIM, which is expected to be farne-sylated. This sequence differs from the wild-type KRas4B CAAX only at the underlined alanine, which represents an S>A mutation. This mutation was made to prevent endogenous regulation at this residue, as previously reported (46). PAmCh-BRAF(G469A) was created by site-directed mutagenesis of PAmCh-BRAF, a generous gift from Eric Collison (UCSF), using the QuikChange Lightning kit (Agilent). For optoBRAF, a YFP-PIF-BRAF was created by PCR amplification of the YFP-PIF-SOS2cat vector backbone to exclude S0S2cat, PCR amplification of wtBRAF, and ligation using the In-Fusion enzyme cocktail (Clontech). Lentivirus was packaged by co transfecting the transfer vector, pCMVdR8.91, and pMD2.G (Addgene # 12259) into Lenti-X 293T cells (Clontech) using the Fugene 6 HD transfection reagent. 48 hours after transfection, viral supernatant was harvested, sterile filtered through a 0.45 μm filter, and added to cells for infection. Unused supernatant was stored at −80°C. 72 hours after infection, transduced cells were sorted for expression using a FACS Aria Fusion (BD Biosciences).

Cell lines, cell culture, and inhibitors

All cell lines were maintained in standard tissue culture incubators at 37° C and 5% CO_2. NIH 3T3s (ATCC) were cultured in DMEM supplemented with 10% calf serum (HyClone) and 1% penicillin/streptomycin/glutamine (ThermoFisher # 10378016). Lenti-X 293T cells were cultured in DMEM High Glucose H-21 (UCSF Cell Culture Facility) supplemented with 10% FBS (UCSF Cell Culture Facility) and 1% penicillin/streptomycin (UCSF Cell Culture Facility). All other lines were cultured in RPMI (UCSF Cell Culture Facility) supplemented with 10% FBS and 1% penicillin/ streptomycin/glutamine. The Mek inhibitors U0126 (Selleckchem #S1102) and trametinib (Selleckchem #S2673) and B-Raf inhibitors vemurafenib (Selleckchem #S1267) and SB590885 (Selleckchem #S2220) were obtained from Selleckchem. PLX-8394 was obtained as a gift from Plexxicon.

Optogenetic stimulation

For all optogenetic experiments, cells were supplemented with HPLC-purified phycocyanobilin (PCB, Frontier Scientific #P14137) at a concentration of 5 μM (3T3s) or 10 μM (all other cells). Cells were incubated in PCB for ~0.5–1 hour before optogenetic stimulation. For bulk Western blot experiments, cells were illuminated in a cell culture incubator with a custom built panel of either 650 nm or 750 nm LEDs for activation or inactivation of optoSOS, respectively. For 96- and 384-well In-Cell Western and immunofluorescence assays, optogenetic experiments were performed with a custom-built 96-well “optoPlate” illuminator with adapters accommodating either 96- or 384- well plates (see fig. S1). Briefly, a printed circuit board was designed using the Kicad software package

Author Manuscript Author Manuscript Author Manuscript Author Manuscript

and manufactured through PCBUnlimited (PCBUnlimited.com). The circuit board design allowed placement of 192 independently addressable LEDs, with two LEDs—one red (Vishay, VLMK31R1S2-GS18), one far-red (Marubeni, SMT780)—fitting under each well position. The LEDs shared a common anode, and each cathode was connected to one of 12 24-channel constant- current LED drivers (TLC5947, Texas Instruments). These drivers allow independent 12-bit grayscale control (0–4095) of each LED using pulse-width modulation. LED drivers were controlled by an on-board Arduino Micro microcontroller, which was programmed with custom script through the Arduino IDE. Custom adapters interfacing with 96- and 384-well plates were designed in the Autodesk Inventor program and printed on a Stratasys uPrint 3D printer.

Western blot

Cells were seeded in 6-well plates at a density of 1×10^5 cells per well. After 24h, cells were starved in starvation medium (DMEM or RPMI media supplemented with 1% penicillin/streptomycin/glutamine, and 20 mM HEPES). Cells were lysed in ice-cold RIPA buffer supplemented with protease (cOmplete, Sigma #4693159001) and phosphatase inhibitors (PhosSTOP, Sigma #4906845001). After a 10 min centrifugation at 4°C, supernatants were supplemented with 5X Laemmli's sample buffer and were boiled for 10 min. SDS PAGE was performed in with in NuPAGE Bis-Tris gels (Invitrogen) using MES buffer (ThermoFisher #NP0002), and blots were transferred onto nitrocellulose membranes using the BioRad Trans-Blot Semi-Dry Transfer Cell. Transferred blots were then blocked with Odyssey blocking buffer (LI-COR #927–4000) and antibody stained using the Freedom Rocker liquid handling system. Western blots were imaged on a LI-COR Odyssey imager, and images were quantified using ImageJ. Phospho-Erk antibody was obtained from Cell Signaling Technologies (#4370), alpha- tubulin antibody was obtained from Santa Cruz Biotechnology (Santa Cruz, #23948,1:1000), and IRDye conjugated secondary antibodies (#926–3221, #926–68020) were obtained from LI-COR.

96- and 384-well optogenetic experiments

Cell seeding, starvation, and illumination—96- or 384-well plates (Greiner #655087 and #781092) were coated in fibronectin (Millipore, #FC010,1:50 dilution in PBS) for 30 min in the incubator. Cells were seeded at 5000 or 1000 cells per well for 96- or 384-well experiments, respectively, and were spun down in the plate for 1 min at 100 X gimmediately after seeding to obtain an even spatial distribution of cells. After 24h, cells were starved with starvation medium (basal medium with 1% penicillin/streptomycin/glutamine and 20 mM HEPES). To balance effective starvation while minimizing loss of cells, cells in 96- well experiments underwent one full medium replacement followed by 4X 70% replacements, performed manually. Cells in 384-well experiments underwent 7X 70% starvation washes with the Biomek FX liquid handling robot. After starvation for 24 hours (signaling experiments) or 36 hours (growth experiments), cells were supplemented with phycocyanobilin (PCB) by mixing a 2X PCB solution in starvation media, removing starvation media from the plate manually, and adding the appropriate amount of 2X PCB. Cells in PCB were then incubated in the dark for 30 min. Any additional drugs were added at the same time and in the same solution as the PCB, with the exception of Mek-i addition in the experiment described in fig. S9. All manipulations with cells in PCB were done under

Author Manuscript Author Manuscript Author Manuscript Author Manuscript

dim light settings, and cell-containing plates were covered with aluminum foil whenever possible to prevent unintended photoactivation. The plates were then placed onto a pre-programmed optoPlate device and exposed to the desired illumination profiles.

Cell fixation, immunostaining, and antibodies—Upon completion of the experiment, cells were immediately supplemented with 16% PFA to a final concentration of 4%PFA. After fixing for 10 min, the PFA-containing medium was manually aspirated with a multichannel pipette and cells were permeabilized with 0.5% Triton X-100 (Sigma) for 10 min followed by ice-cold 100% methanol at −20°C for 10 min. Cells were then blocked for 30 min at room temperature with Odyssey Blocking Buffer (LI-COR). Primary antibodies were then diluted in fresh blocking buffer: anti-ppErk (CST #4370,1:200), anti-ppErk(CST # 4344,1:50), anti-cJun (CST #9165,1:100), anti- EGR1 (CST #4154,1:800), anti-CyclinD1 (Abcam #ab134175,1:100). Blocking buffer was removed and cells were incubated in primary antibody solutions overnight. Cells were washed 5X with PBS with 0.1% Tween-20 (Sigma). All washes were performed with a BioTek EL406 liquid handler. Cells were then incubated in secondary antibody solutions. For In-Cell Western experiments, IRDye 800CW-conjugated goat anti-Rabbit (Licor, #926–32211,1:800) secondary was used, and CellTag700 (Licor, #926–41090,1:2000) was used for normalization. For single cell immunofluorescence, Alexa-488 and Alexa-647 conjugated goat anti-Rabbit secondary antibodies (Jackson Immunoresearch, #111–545-003 and #111–605-003, 1:100) were used in conjunction with DAPI (Molecular Probes, #D1306,300 nM) for nuclear labeling. After 1 hour of secondary antibody incubation, cells were washed 5X in PBS + 0.1% Tween-20.

Imaging—In-Cell Western: For In-Cell Western experiments, plates were imaged on the LI-COR Odyssey scanner. Intensity measurements for each well were exported using the integrated In-Cell Western analysis software and were further analyzed in R.

High content imaging: Single cell immunofluorescence and Edu labeling (below) was measured on the ThermoFisher Scientific ArrayScan XTI High Content Platform imager, and image quantitation was conducted through the integrated HCS Studio software. Briefly, cells were identified through segmentation of DAPI-stained nuclei, and parameters were specified to ensure proper segmentation of single cells. Mean nuclear intensities were then calculated for each cell for the fluorescence channels reporting on all targets except for ppErk. For ppErk, a 2–5 pixel-wide ring was drawn around the nucleus, and mean fluorescence intensity in this ring was recorded. The fluorescence measurements were then exported, and further analysis was conducted in R.

Edu proliferation assay

S-phase entry was assessed through Edu incorporation using the Click-iT Edu AlexaFluor 555 Imaging kit (ThermoFisher, #C10338). Cells were seeded and starved as described above in the “96- and 384-well optogenetics experiments” section. After completion of the desired illumination time, cells were supplemented with a 30 min Edu pulse (5 μM) for 30 additional minutes of illumination. Cells were then fixed and permeabilized as described, and Edu was conjugated to AlexaFluor 555 as per manufacturer instructions.

Author Manuscript Author Manuscript Author Manuscript Author Manuscript

Live cell microscopy

Cells were seeded in 384 well glass bottom plates (Matrical, Inc. #MGB101–1-2-LG) that were pre-coated with 50 uL of 20 μg/mL fibronectin (Millipore # FC010) for 1 hour. Upon seeding, cells were spun down at 100 × g for 1 min to promote an even distribution of cells on the well bottom. The following day, cells were starved with starvation medium (defined above). 1 hour before imaging, starvation medium was replaced with fresh starvation medium containing 5 μM PCB.

Confocal imaging was conducted on a Nikon Eclipse TI inverted microscope with a Yokagawa CSU-X1 spinning disk confocal unit, a 20× PlanApo TIRF 1.49 NA objective, and an EM-CCD camera (Andor). Environmental control was maintained with a humidified environmental chamber at 37°C and 5% CO_2 (In Vivo Scientific). BFP, YFP, and mCherry were imaged with 405 nm, 488 nm, and 561 nm lasers (LMM5, Spectral Applier Research), respectively.

Cells were exposed to 650 nm and 750 nm light for optogenetic control as described previously (16). Briefly, a 650 nm LED was mounted into the epifluorescence illumination port, and its light intensity (voltage control) was regulated with custom Matlab scripts (45) controlling the analog output of a DT9812 board (Data Translation), which was connected to the LED. 750 nm light was applied by filtering bright-field light through a 750 nm longpass filter (FSQ-RG9, Newport) and controlling its timing through software control of the diascopic shutter.

Image analysis

BFP-Erk2 responses to variable Ras input pulses—For visualizing BFP-Erk2 responses to dynamic Ras activation, live cell imaging was analyzed with a combination of ImageJ and custom R scripts. Nuclear accumulation of BFP-Erk2 was measured by mean fluorescence intensity of an ROI within the cell nucleus in the BFP channel, and YFP-PIF-SOS2cat membrane translocation was measured by cytoplasmic depletion of YFP, as described previously (16). BFP and YFP traces for individual cells were then corrected for fluorescence drift. Traces underwent a linear transform by calculating a linear regression of all points, and then subtracting this fit from the original trace. Photobleaching was corrected by fitting an exponential decay envelope to each trace and dividing each trace by its envelope function. Traces were then normalized between 0 and 1, and the YFP-SOS2cat trace was inverted for visual clarity.

Edu and immunofluorescence analysis—For quantifying the fraction of Edu+ cells in a well, density plots of Edu intensities of cells in each well were constructed. The Edu distribution was bimodal, with a tight peak for Edu- cells and a broader peak for Edu+ cells. A custom segmentation algorithm classified the Edu- and Edu+ populations for each trace. Example peaks and segmentation are shown in Fig. S12C.

For single cell immunofluorescence, fluorescence distributions were generated for each well and the distribution median was extracted.

Author Manuscript Author Manuscript Author Manuscript Author Manuscript

Model and fitting

Low pass filter of signal processing—To model how cells filter and respond to signals, we constructed a 3-step model. The first step describes signal filtering, the second describes signal perception, and the third describes cell fate decisions resulting from that perception.

To model low-pass signal filtering, we implemented a conceptually simple filter, a first-order RC circuit. This model consists of a voltage source V, resistor R, and capacitor C wired in series. In our example, these can be thought of as the input signal, signal transduction through the pathway, and the ability for the cell to hold that signal (e.g., the total abundance of a protein that can be activated), respectively. We were interested in measuring the voltage (signal) across the capacitor ($V_C = q/C$) as a function of dynamic inputs. Kirchoff s voltage law states that the sum of the voltages across each component in this loop equals 0

$$V - V_R - V_C = 0$$
$$V(t) - \frac{dq(t)}{dt}R - \frac{q(t)}{C} = 0$$

where $C = 1$, R was variably defined, and V was the dynamic model input. Dynamic inputs were achieved by changing the value of V between 0 (OFF) and 1 (ON) at defined intervals.

The time constants $\tau = RC$ define the signal kinetics in this model, which describe the speed of exponential rise and decay of the signal. To model signal processing changes in cancer, we changed the value of R, thus changing the value of t. We started the simulation from a state of rest, where $q(t = 0) = 0$. We implemented the model in the R programming language (https://cran.r-project.org) using the deSolve package.

To model cellular perception of a filtered signal, we defined a signal intensity at which downstream transcriptional circuits are turned on. In fig. S10, B and C, we defined this threshold to be 30% based on estimates from previous studies (2, 47), but fig. S10D shows that a broad range of threshold values gives qualitatively similar results.

Finally, we assumed that a cell's decision to proliferate was directly correlated to the cumulative signal the cell perceived by the end of the simulation. Many possible relationships exist between perceived signal and proliferation, but we chose a direct correlation due to its simplicity. We expect that a different relationship would also show that altered signal perception could lead to differential cell fate choices, though the set of inputs subject to misperception may change.

Curve fitting—Single exponential decay was fitted to normalized kinetics data using the *glm* function in R assuming a Gaussian error distribution and a "log" linkage. The curves describing proliferation as a function of duty cycle in Fig. S12F were fit to a Hill function.

Supplementary Material

Refer to Web version on PubMed Central for supplementary material.

Author Manuscript Author Manuscript Author Manuscript Author Manuscript

ACKNOWLEDGMENTS

We thank G. Bollag and Plexxikon for providing PLX8394 and N. Frankel and G. Bollag for critical reading and comments on the manuscript. We also thank N. Repina (University of California, Berkeley) for helpful discussions on optogenetic device design, E. Chow for discussions on device construction, A. Meyer-Franke for technical help with high-content microscopy, and A. Basu (Wayne State University) for providing an alternative device for multiwell optogenetic experiments. **Funding:** This work was funded by the Arnold O. Beckman Postdoctoral Fellowship (L.J.B.); the European Molecular Biology Organization ALTF 419-2010 (A.M.); the UCSF Program for Breakthrough Biomedical Research Postdoctoral Research Award (A.M.); NIH DP2EB024247 (J.E.T.); St. Baldrick's Foundation and a Damon Runyon-Sohn Foundation fellowship 6P-13 (A.S.); NIH DP2 CA174497, R01CA169338, R01CA204302, and R01CA211052 (T.G.B); the Pew and Stewart Foundations (T.G.B.); the Howard Hughes Medical Institute (W.A.L); and NIH P50GM081879 and R01GM55040 (W.A.L.).

REFERENCES AND NOTES

1. Shaul YD, Seger R, The MEK/ERK cascade: From signaling specificity to diverse functions. Biochim. Biophys. Acta 1773, 1213–1226 (2007). [PubMed: 17112607]
2. Albeck JG, Mills GB, Brugge JS, Frequency-modulated pulses of ERK activity transmit quantitative proliferation signals. Mol. Cell 49, 249–261 (2013). doi: 10.1016/j.molcel.2012.11.002 [PubMed: 23219535]
3. Aoki K et al., Stochastic ERK activation induced by noise and cell-to-cell propagation regulates cell density-dependent proliferation. Mol. Cell 52, 529–540 (2013). doi: 10.1016/j.molcel.2013.09.015 [PubMed: 24140422]
4. Hiratsuka T et al., Intercellular propagation of extracellular signal-regulated kinase activation revealed by in vivo imaging of mouse skin. eLife 4, e05178 (2015). doi: 10.7554/eLife.05178 [PubMed: 25668746]
5. Marshall CJ, Specificity of receptor tyrosine kinase signaling: Transient versus sustained extracellular signal-regulated kinase activation. Cell 80, 179–185 (1995). doi: 10.1016/0092-8674(95)90401-8 [PubMed: 7834738]
6. Rauch N, Rukhlenko OS, Kolch W, Kholodenko BN, MAPK kinase signalling dynamics regulate cell fate decisions and drug resistance. Curr. Opin. Struct. Biol 41, 151–158 (2016). doi: 10.1016/j.sbi.2016.07.019 [PubMed: 27521656]
7. Behar M, Dohlman HG, Elston TC, Kinetic insulation as an effective mechanism for achieving pathway specificity in intracellular signaling networks. Proc. Natl. Acad. Sci. U.S.A 104, 16146–16151 (2007). doi: 10.1073/pnas.0703894104 [PubMed: 17913886]
8. Cohen-Saidon C, Cohen AA, Sigal A, Liron Y, Alon U, Dynamics and variability of ERK2 response to EGF in individual living cells. Mol. Cell 36, 885–893 (2009). doi: 10.1016/j.molcel.2009.11.025 [PubMed: 20005850]
9. Kellogg RA, Tay S, Noise facilitates transcriptional control under dynamic inputs. Cell 160, 381–392 (2015). doi: 10.1016/j.cell.2015.01.013 [PubMed: 25635454]
10. Santos SDM, Verveer PJ, Bastiaens PIH, Growth factor-induced MAPK network topology shapes Erk response determining PC-12 cell fate. Nat. Cell Biol 9, 324–330 (2007). doi: 10.1038/ncb1543 [PubMed: 17310240]
11. Hao N, O'Shea EK, Signal-dependent dynamics of transcription factor translocation controls gene expression. Nat. Struct. Mol. Biol 19, 31–39 (2011). doi: 10.1038/nsmb.2192 [PubMed: 22179789]
12. Purvis JE et al., p53 dynamics control cell fate. Science 336, 1440–1444 (2012). doi: 10.1126/science.1218351 [PubMed: 22700930]
13. Purvis JE, Lahav G, Encoding and decoding cellular information through signaling dynamics. Cell 152, 945–956 (2013). doi: 10.1016/j.cell.2013.02.005 [PubMed: 23452846]
14. Selimkhanov J et al., Accurate information transmission through dynamic biochemical signaling networks. Science 346,1370–1373 (2014). doi: 10.1126/science.1254933 [PubMed: 25504722]
15. Ashall L et al., Pulsatile stimulation determines timing and specificity of NF-kB-dependent transcription. Science 324, 242–246 (2009). doi: 10.1126/science.1164860 [PubMed: 19359585]

Author Manuscript Author Manuscript Author Manuscript Author Manuscript

16. Toettcher JE, Weiner OD, Lim WA, Using optogenetics to interrogate the dynamic control of signal transmission by the Ras/Erk module. Cell 155,1422–1434 (2013). doi: 10.1016/j.cell.2013.11.004 [PubMed: 24315106]
17. Murphy LO, MacKeigan JP, Blenis J, A network of immediate early gene products propagates subtle differences in mitogen-activated protein kinase signal amplitude and duration. Mol. Cell. Biol 24, 144–153 (2004). doi: 10.1128/MCB.24.1.144-153.2004 [PubMed: 14673150]
18. Murphy LO, Smith S, Chen R-H, Fingar DC, Blenis J, Molecular interpretation of ERK signal duration by immediate early gene products. Nat. Cell Biol 4, 556–564 (2002). doi: 10.1038/ncb822 [PubMed: 12134156]
19. Uhlitz F et al., An immediate-late gene expression module decodes ERK signal duration. Mol. Syst. Biol 13, 928 (2017). doi: 10.15252/msb.20177554 [PubMed: 28468958]
20. Roberts PJ, Der CJ, Targeting the Raf-MEK-ERK mitogen-activated protein kinase cascade for the treatment of cancer. Oncogene 26, 3291–3310 (2007). doi: 10.1038/sj.onc.1210422 [PubMed: 17496923]
21. Burack WR, Shaw AS, Live cell imaging of ERK and MEK: Simple binding equilibrium explains the regulated nucleocytoplasmic distribution of ERK. J. Biol. Chem. 280, 3832–3837 (2005). doi: 10.1074/jbc.M410031200 [PubMed: 15546878]
22. Zhang C et al., RAF inhibitors that evade paradoxical MAPK pathway activation. Nature 526, 583–586 (2015). doi: 10.1038/nature14982 [PubMed: 26466569]
23. Zhang K et al., Light-mediated kinetic control reveals the temporal effect of the Raf/MEK/ERK pathway in PC12 cell neurite outgrowth. PLOS ONE 9, e92917 (2014). doi: 10.1371/journal.pone.0092917 [PubMed: 24667437]
24. Brummer T, Naegele H, Reth M, Misawa Y, Identification of novel ERK-mediated feedback phosphorylation sites at the C-terminus of B-Raf. Oncogene 22, 8823–8834 (2003). doi: 10.1038/sj.onc.1207185 [PubMed: 14654779]
25. Ritt DA, Monson DM, Specht SI, Morrison DK, Impact of feedback phosphorylation and Raf heterodimerization on normal and mutant B-Raf signaling. Mol. Cell. Biol 30, 806–819 (2010). doi: 10.1128/MCB.00569-09 [PubMed: 19933846]
26. Wan PT et al., Mechanism of activation of the RAF-ERK signaling pathway by oncogenic mutations of B-RAF. Cell 116, 855–867 (2004). doi: 10.1016/S0092-8674(04)00215-6 [PubMed: 15035987]
27. Garnett MJ, Rana S, Paterson H, Barford D, Marais R, Wild-type and mutant B-RAF activate C-RAF through distinct mechanisms involving heterodimerization. Mol. Cell 20, 963–969 (2005). doi: 10.1016/j.molcel.2005.10.022 [PubMed: 16364920]
28. Yao Z et al., BRAF mutants evade ERK-dependent feedback by different mechanisms that determine their sensitivity to pharmacologic inhibition. Cancer Cell 28, 370–383 (2015). doi: 10.1016/j.ccell.2015.08.001 [PubMed: 26343582]
29. Poulikakos PI, Zhang C, Bollag G, Shokat KM, Rosen N, RAF inhibitors transactivate RAF dimers and ERK signalling in cells with wild-type BRAF. Nature 464, 427–430 (2010). doi: 10.1038/nature08902 [PubMed: 20179705]
30. Rajakulendran T, Sahmi M, Lefranpois M, Sicheri F, Therrien M, A dimerization-dependent mechanism drives RAF catalytic activation. Nature 461, 542–545 (2009). doi: 10.1038/nature08314 [PubMed: 19727074]
31. Hatzivassiliou G et al., RAF inhibitors prime wild-type RAF to activate the MAPK pathway and enhance growth. Nature 464, 431–435 (2010). doi: 10.1038/nature08833 [PubMed: 20130576]
32. Heidorn SJ et al., Kinase-dead BRAF and oncogenic RAS cooperate to drive tumor progression through CRAF. Cell 140, 209–221 (2010). doi: 10.1016/j.cell.2009.12.040 [PubMed: 20141835]
33. Chapman PB et al., Improved survival with vemurafenib in melanoma with BRAF V600E mutation. N. Engl. J. Med 364, 2507–2516 (2011). doi: 10.1056/NEJMoa1103782 [PubMed: 21639808]
34. Flaherty KT et al., Inhibition of mutated, activated BRAF in metastatic melanoma. N. Engl. J. Med 363, 809–819 (2010). doi: 10.1056/NEJMoa1002011 [PubMed: 20818844]

Author Manuscript Author Manuscript Author Manuscript Author Manuscript

35. Larkin J et al., Vemurafenib in patients with BRAF(V600) mutated metastatic melanoma: An open-label, multicentre, safety study. Lancet Oncol. 15, 436–444 (2014). doi: 10.1016/S1470-2045(14)70051-8 [PubMed: 24582505]
36. Su F et al., RAS mutations in cutaneous squamous-cell carcinomas in patients treated with BRAF inhibitors. N. Engl. J. Med 366, 207–215 (2012). doi: 10.1056/NEJMoa1105358 [PubMed: 22256804]
37. Tian T et al., Plasma membrane nanoswitches generate high-fidelity Ras signal transduction. Nat. Cell Biol 9, 905–914 (2007). doi: 10.1038/ncb1615 [PubMed: 17618274]
38. Cho KJ et al., Raf inhibitors target ras spatiotemporal dynamics. Curr. Biol 22, 945–955 (2012). doi: 10.1016/j.cub.2012.03.067 [PubMed: 22560614]
39. Kumbrink J, Gerlinger M, Johnson JP, Egr-1 induces the expression of its corepressor nab2 by activation of the nab2 promoter thereby establishing a negative feedback loop. J. Biol. Chem 280, 42785–42793 (2005). doi: 10.1074/jbc.M511079200 [PubMed: 16260776]
40. Sparta B et al., Receptor level mechanisms are required for epidermal growth factor (EGF)-stimulated extracellular signal-regulated kinase (ERK) activity pulses. J. Biol. Chem 290, 24784–24792 (2015). doi: 10.1074/jbc.M115.662247 [PubMed: 26304118]
41. Bugaj LJ, O'Donoghue GP, Lim WA, Interrogating cellular perception and decision making with optogenetic tools. J. Cell Biol 216, 25–28 (2017). doi: 10.1083/jcb.201612094 [PubMed: 28003330]
42. Lee MJ et al., Sequential application of anticancer drugs enhances cell death by rewiring apoptotic signaling networks. Cell 149, 780–794 (2012). doi: 10.1016/j.cell.2012.03.031 [PubMed: 22579283]
43. Chen SH, Forrester W, Lahav G, Schedule-dependent interaction between anticancer treatments. Science 351, 1204–1208 (2016). doi: 10.1126/science.aac5610 [PubMed: 26965628]
44. Behar M, Barken D, Werner SL, Hoffmann A, The dynamics of signaling as a pharmacological target. Cell 155, 448–461 (2013). doi: 10.1016/j.cell.2013.09.018 [PubMed: 24120141]
45. Toettcher JE, Gong D, Lim WA, Weiner OD, Light-based feedback for controlling intracellular signaling dynamics. Nat. Methods 8, 837–839 (2011). doi: 10.1038/nmeth.1700 [PubMed: 21909100]
46. Bivona TG et al., PKC regulates a farnesyl-electrostatic switch on K-Ras that promotes its association with Bcl-XL on mitochondria and induces apoptosis. Mol. Cell 21, 481–493 (2006). doi: 10.1016/j.molcel.2006.01.012 [PubMed: 16483930]
47. Bollag G et al., Clinical efficacy of a RAF inhibitor needs broad target blockade in BRAF-mutant melanoma. Nature 467, 596–599 (2010). doi: 10.1038/nature09454 [PubMed: 20823850]

Author Manuscript Author Manuscript Author Manuscript Author Manuscript

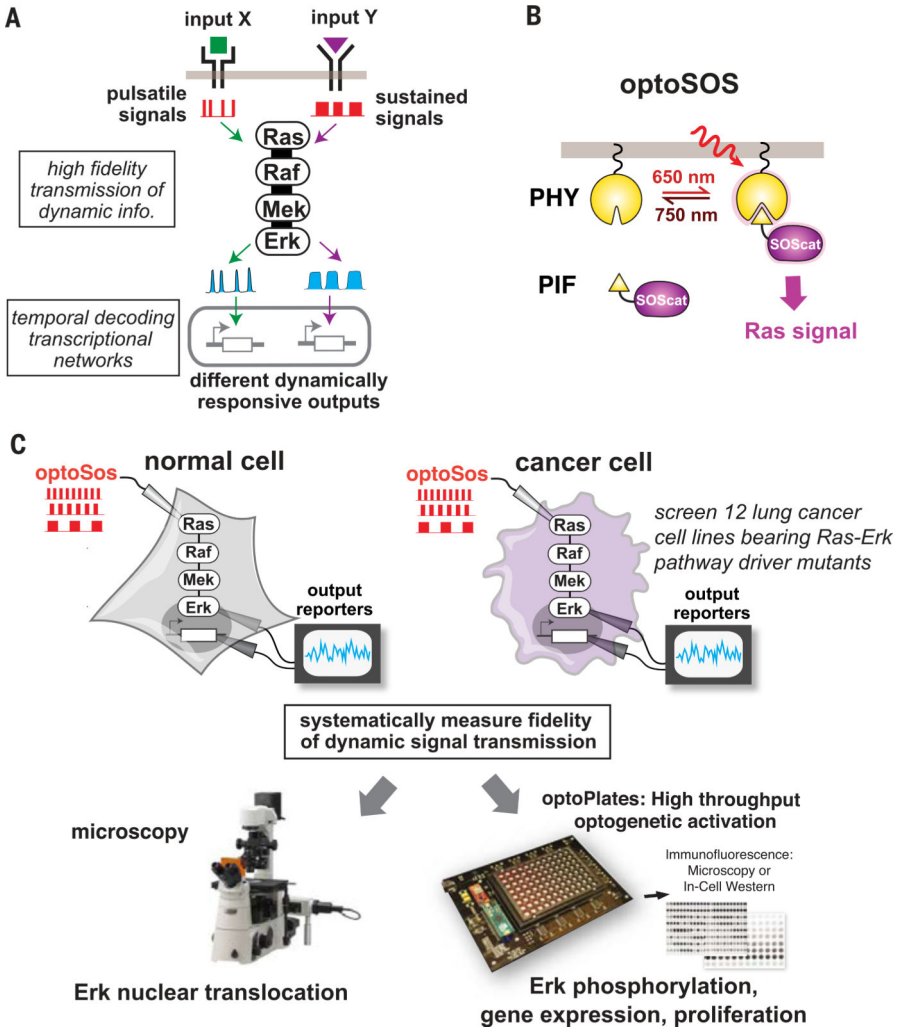

Fig. 1. Probing dynamic signal transduction and filtering in cancer cells.

(**A**) Environmental stimuli can induce different dynamic patterns of Erk activity, which are then interpreted by downstream transcriptional circuits to specify cell behavior. (**B**) OptoSOS is an optogenetic method for Ras activation that enables probing of how cells filter and respond to dynamic Ras inputs. The light-inducible PhyB-PIF heterodimer drives membrane recruitment of the Ras-activating SOS2 catalytic domain, which activates Ras at the membrane. Red light (650 nm) induces PhyB-PIF dimerization, whereas far-red light (750 nm) dissociates the dimer. (**C**) We tested the hypothesis that some cancer cells may inappropriately filter dynamic Ras-Erk signals. We examined how dynamic optogenetic inputs were interpreted by normal or cancer cells through a combination of live-cell microscopy, high-throughput optogenetic stimulation (fig. S1), and immunofluorescence.

Author Manuscript Author Manuscript Author Manuscript Author Manuscript

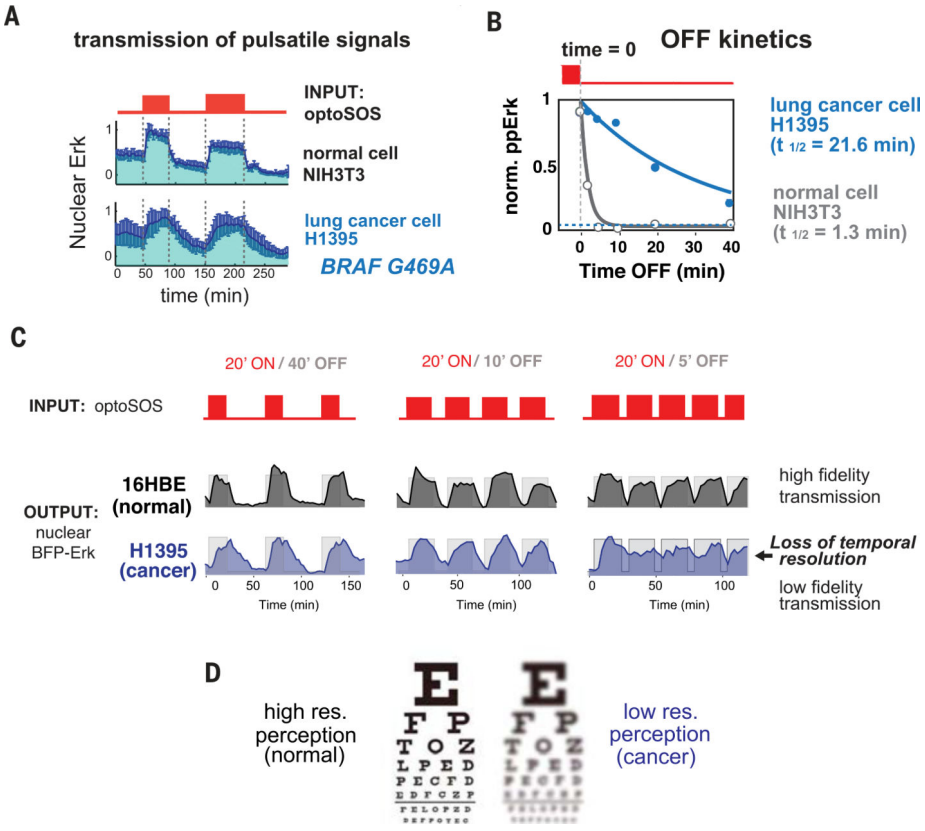

Fig. 2. B-Raf mutant H1395 cells have an impaired transmission of pulsatile Ras signals.

(**A**) H1395 cells (bottom) showed extended kinetics of activation and inactivation in response to defined Ras input pulses. By contrast, NIH 3T3 cells (top) and the other cells in our cell line panel exhibited rapid kinetics (fig. S2B). Traces represent quantitation from live-cell imaging of nuclear BFP-Erk2 reporter accumulation. Traces were normalized between 0 and 1 and represent the mean ± 1 SD of 15 and 14 cells for 3T3 and H1395 cells, respectively. (**B**) Inactivation kinetics for H1395 and NIH 3T3 cells were confirmed through Western blot (blots are available in fig. S3A). Western blot quantification of ppErk is shown and fitted to single exponential decay.The dashed blue line depicts basal amount of ppErk from unstimulated cells. (**C**) Loss of fidelity in dynamic signal transduction in H1395 cells was observed through live-cell microscopy. 16-HBE (normal) and H1395 (cancer) cells were subjected to various dynamic patterns of input signal. (Three input conditions are shown. All six input conditions are shown in fig. S3B). As optoSOS input frequency increased, the H1395 cancer cells progressively lost their response to the gaps in the signal, whereas the normal cells did not. Traces represent the mean of five cells. Individual traces can be seen in fig. S3B. (**D**) Changes in the cell's signal perception are analogous to cellular "blurred vision" for external stimuli. (Single-letter abbreviations for the amino acid residues are as follows: A, Ala; G, Gly; and V, Val. In the mutants, other amino acids were substituted at certain locations; for example, G469A indicates that glycine at position 469 is replaced by alanine.)

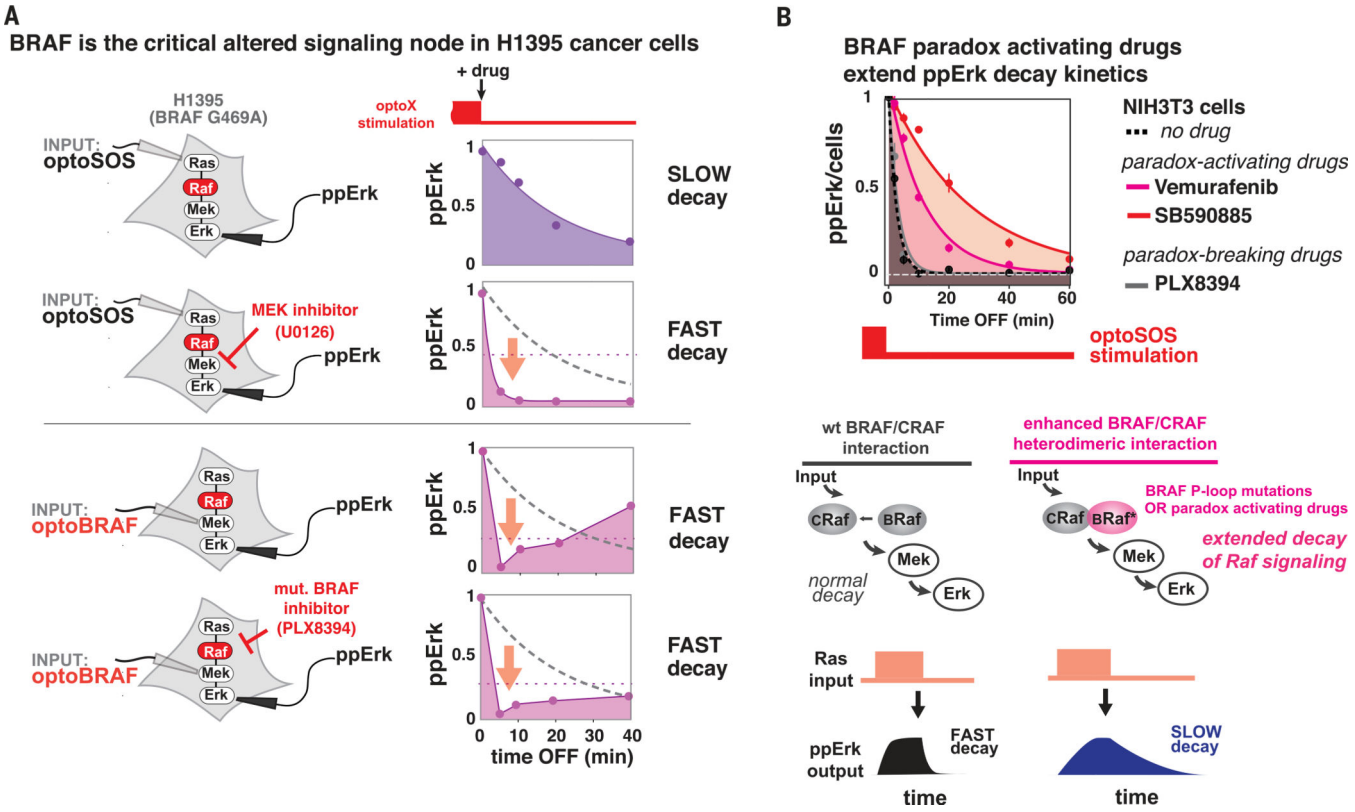

Fig. 3. B-Raf P-loop mutations and drugs that perturb Raf dimerization both extend Ras-Erk pathway kinetics.

(**A**) OptoSOS and optoBRaf coupled with MEK inhibition (U0126) and mutant-B-Raf inhibition (PLX-8394) were used to isolate B-Raf as a network node that can extend Erk kinetics. Plots show quantification of Western blot data (blots are available in fig. S4, A, B, and C). Normal wild-type decay is indicated with the gray dashed line; basal signaling level (no opto-stimulation) is indicated by the purple dotted line. (**B**) Treatment of NIH 3T3s with paradoxically activating B-Raf inhibitors vemurafenib and SB590885 also extended ppErk decay kinetics. Datapoints show means ± 95% confidence interval (CI) of mean single-cell ppErk immunofluoresecnce from three replicates. (**C**) Our data support a model in which P-loop B-Raf mutations or paradoxically activating drugs can both enhance the Ras-induced dimerization potential of B-Raf and C-Raf, thus altering the kinetic properties of pathway activation and inactivation.

Author Manuscript Author Manuscript Author Manuscript Author Manuscript

Author Manuscript Author Manuscript Author Manuscript Author Manuscript

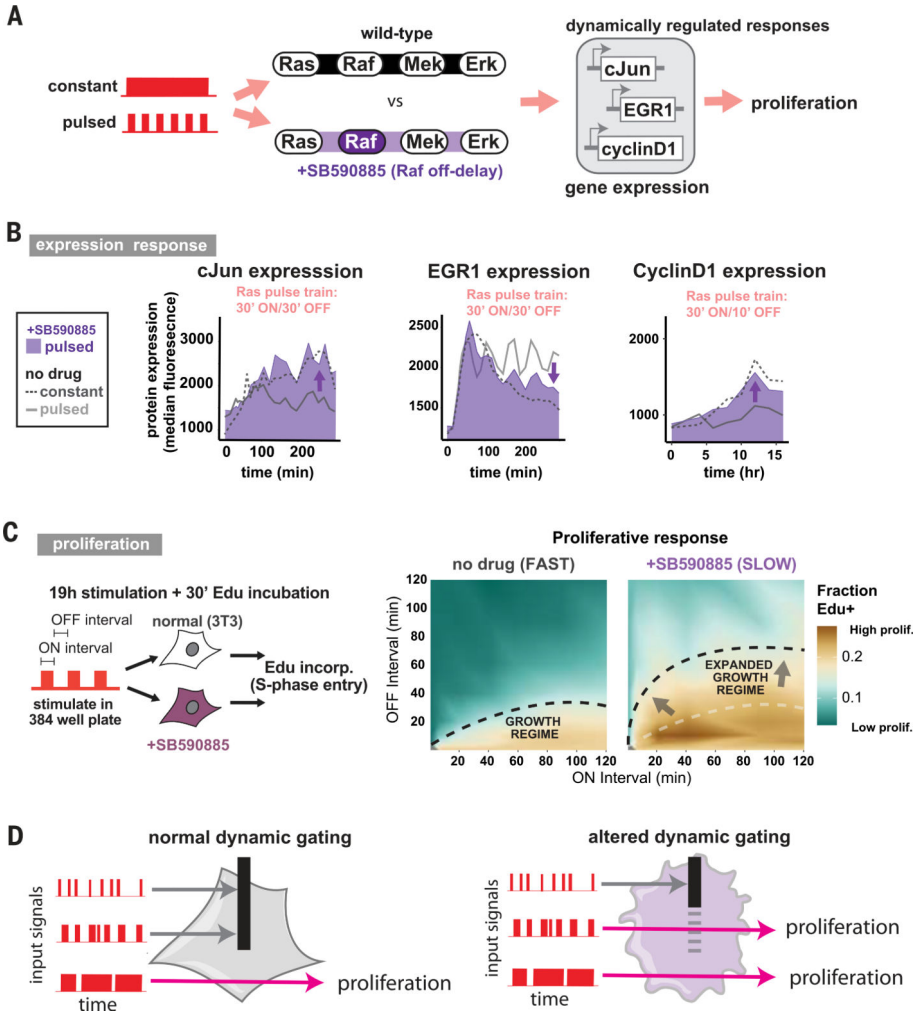

Fig. 4. Perturbation of Ras-Erk signaling dynamics can alter how cells make proliferative decisions.

(**A**) Transcriptional decoding of dynamic signal inputs was examined in normal NIH 3T3 cells (fast pathway kinetics) or in cells treated with the kinetics-altering drug SB590885. Cells were stimulated with fixed-width signal pulses separated by various intervals. Expression of Erk targets and downstream cell-cycle entry were examined. (**B**) Altered Ras-Erk kinetics changed transcriptional output to dynamic Ras inputs. Immunofluorescence of cJun, EGR1, and Cyclin D1 expression time courses is depicted. Only expression in response to constant stimulus or a representative pulsed stimulus is shown.All input conditions tested are provided in fig. S11. Illumination was achieved with the optoPlate, and protein expression was assessed through single-cell immunofluorescence coupled with high-content imaging. Data points represent the median target fluorescence from 3000 to 4000 cells for each condition. (**C**) Extended Ras-Erk kinetics sensitized cells to proliferate under nonproliferative conditions. We used 384-well optoPlate illumination to examine proliferation of cells in response to a systematic scan of dynamic inputs. Normal and drug-treated cells were exposed to all combinations of six optoSOS pulse lengths (ON interval) and separated by seven pulse interval lengths (OFF interval) over 19 hours. Cells were then incubated with Edu for 30 min, fixed, stained, imaged, and analyzed. The percentage of cells

Author Manuscript Author Manuscript Author Manuscript Author Manuscript

incorporating Edu was plotted as an interpolated heatmap. Further analysis is available in figs. S12 and S13. The values used to generate the map represent means of biological quadruplicates. (**D**) Our data support the model that altering dynamic signal filtering properties can reshape the input-response map and may drive improper cellular behavior, such as hyperproliferation.